

Robust Optimized Pulse Patterns for Converters Connected to a Distorted Grid via LCL Filters

Shirin Rahmanpour
Faculty of Inf. Technol.
and Commun. Sciences
Tampere University
Tampere, Finland
shirin.rahmanpour@tuni.fi

Petros Karamanakos
Faculty of Inf. Technol.
and Commun. Sciences
Tampere University
Tampere, Finland
p.karamanakos@ieee.org

Tobias Geyer
Motion System Drives
ABB Switzerland Ltd
Turgi, Switzerland
t.geyer@ieee.org

George Papafotiou
Dept. of Electrical Engineering
Eindhoven University of Technology
Eindhoven, the Netherlands
g.papafotiou@tue.nl

Abstract—This paper presents robust harmonic-constrained optimized pulse patterns (OPPs) for converters connected to a distorted grid via LCL filters. Specifically, the proposed OPPs ensure compliance with harmonic grid standards even in the presence of unknown harmonic voltages—treated as disturbances—jected to the point of common coupling (PCC) by other converters. This is achieved by formulating and solving a robust OPP optimization problem that accounts for the impact of disturbances while imposing constraints on individual current and voltage harmonics at the PCC. Numerical results demonstrate the grid-friendly operation of the proposed robust OPPs under disturbance harmonics with magnitudes of up to 55% of the maximum levels allowed by grid standards. As shown, the robust OPPs outperform both conventional OPPs and selective harmonic elimination (SHE) in maintaining compliance with harmonic grid standards, despite the disturbances being unknown in the OPP computation process.

Index Terms—Grid-connected converters, grid standards, harmonic distortion, optimized pulse patterns (OPPs), pulse width modulation (PWM).

I. INTRODUCTION

For grid-connected converters, ensuring that the output current and voltage comply with grid standards is essential to maintaining grid stability and reliability. Standards such as IEEE 519 [1] and IEC 61000-2-4 [2] define limits for individual current and voltage harmonics as well as total demand distortion (TDD) at the point of common coupling (PCC).

To limit the harmonic distortion caused by the switching behavior of power converters, passive harmonic filters are typically employed to attenuate harmonics above the filter resonance frequency, with LCL filters being the most commonly used configuration. However, mitigating low-order harmonics remains a challenge, particularly when operating at switching frequencies close to the filter resonance frequency to reduce switching losses and minimize filter size. To address this limitation, active power filters (APFs) can be used in conjunction with passive filters to help mitigate these harmonics [3]–[7]. This approach, however, tends to increase design complexity and component requirements.

A software-based alternative is the use of programmed pulse width modulation (PWM) techniques, such as selective

harmonic elimination/mitigation (SHE/SHM) [8]–[11] and optimized pulse patterns (OPPs) [12]–[14]. Among these, OPPs demonstrate superior harmonic performance and favorable converter operation [15]–[17], as they are computed based on an optimization problem formulated to minimize the harmonic distortions of the output current, typically under the assumption of an inductive load.

To tailor OPPs to higher-order systems, such as grid-connected converters with LCL filters, [18] incorporates the filter transfer function from the switching signal to the grid current into the OPP optimization problem. As a result, the quality of the grid current is significantly improved. However, this approach does not inherently guarantee compliance with harmonic grid standards. This issue is addressed in [19], where individual harmonic components of grid current are explicitly constrained to meet the limits dictated by relevant standards.

Despite their advantages, the harmonic performance of the aforementioned OPPs can degrade under nonideal grid conditions, e.g., when other converters inject harmonic voltages—hereafter referred to as disturbances—into the PCC. The challenge of shaping the desired harmonic spectrum in the presence of such disturbances is partially investigated in [20], [21], although both works are limited to first-order systems.

For higher-order systems, ensuring compliance with grid standards under disturbances is explored in [22]. That work reformulates the OPP optimization problem to account for the contributions of different harmonic sources—namely, the converter of interest and other converters—to the PCC current and voltage. Nevertheless, [22] assumes that the frequency, magnitude, and phase of disturbance harmonics are fully known, an assumption that rarely holds in real-world scenarios. Consequently, if the actual disturbance profile deviates from that considered during the offline OPP computation, compliance with grid standards can be compromised.

Motivated by the above, this paper reformulates the OPP optimization problem to compute *robust* harmonic-constrained OPPs that ensure the PCC current and voltage harmonics remain within the limits dictated by harmonic grid standards, even in the presence of (unknown) disturbances. As shown, the proposed robust OPPs can ensure this desired behavior for disturbance magnitudes up to 55% of the allowable levels,

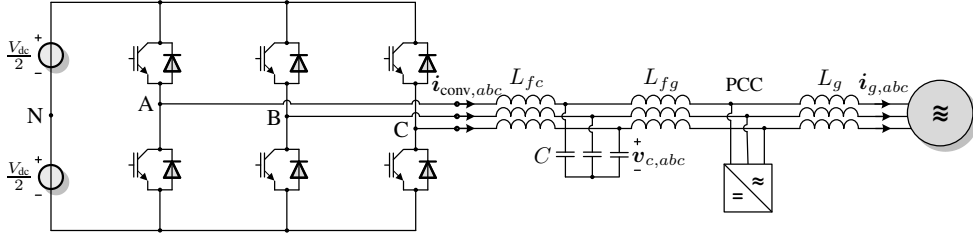


Fig. 1. Two-level converter connected to the grid through an LCL filter. Other converters connected to the PCC introduce additional current and voltage harmonics.

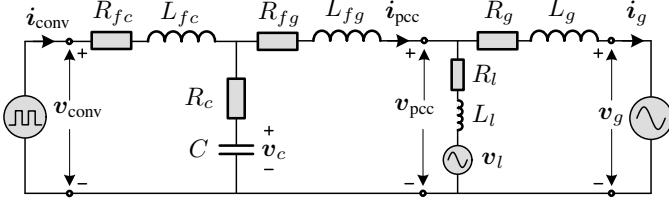


Fig. 2. Equivalent circuit of the system in the $\alpha\beta$ -frame.

regardless of their phase. In contrast, conventional OPPs and SHE fail to achieve such grid-friendly performance, as demonstrated by the presented numerical comparisons.

II. ROBUST OPPS FOR CONVERTERS CONNECTED TO A DISTORTED GRID

OPPs are computed for a low-voltage (LV) power electronic system comprising a two-level converter connected to the grid through an LCL filter (see Fig. 1), while other converters distort the current and voltage at the PCC. In the sequel of this section, the system under study is modeled, and both the conventional and robust OPP optimization problems are formulated.

A. Modeling of the Grid-Connected Converter with LCL Filter

The $\alpha\beta$ -frame equivalent circuit of the system is shown in Fig. 2.¹ To derive the system model, the contributions of different harmonic sources to the current and voltage at the PCC must be investigated separately, while discarding the ripple-free grid voltage v_g . One source of harmonics is the converter of interest, and the other is the aggregate of additional converters connected to the PCC. The latter is represented by the equivalent voltage source v_l connected to the PCC through a transformer with lumped inductance L_l and series resistance R_l , see Fig. 2. It is important to note that the harmonic voltage across the branch corresponding to the other converters at the PCC is modeled as $v_{d,abc}$, consisting of components which are treated as disturbances to the system.

To evaluate the contribution of the converter output voltage v_{conv} , the impact of v_l is neglected by modeling it as a short circuit. Note that v_{conv} is given by

$$v_{conv}(t) = \frac{V_{dc}}{2} \mathbf{K} \mathbf{u}_{abc}(t),$$

¹For notational simplicity, the $\alpha\beta$ subscript is dropped from variables in this frame, while variables in the abc -frame keep their subscripts.

where V_{dc} is the dc-link voltage, $\mathbf{u}_{abc} = [u_a \ u_b \ u_c]^T \in \{-1, 1\}^3$ is the three-phase converter switch position, and \mathbf{K} is the transformation matrix from the three-phase (abc) frame to the stationary orthogonal ($\alpha\beta$) frame.

With v_l short-circuited, the state-space model that describes the system dynamics can be derived.² In doing so, and by using the Laplace transform, the transfer matrices $\mathbf{M}_I(s)$ and $\mathbf{M}_V(s)$ from the converter switch position \mathbf{u}_{abc} to the three-phase PCC current $\mathbf{i}_{pcc,1,abc}$ and voltage $\mathbf{v}_{pcc,1,abc}$, respectively, are obtained in the frequency domain, i.e.,

$$\mathbf{M}_I(s) = \mathcal{L}\{\mathbf{i}_{pcc,1,abc}\}(s) / \mathcal{L}\{\mathbf{u}_{abc}\}(s),$$

$$\mathbf{M}_V(s) = \mathcal{L}\{\mathbf{v}_{pcc,1,abc}\}(s) / \mathcal{L}\{\mathbf{u}_{abc}\}(s).$$

In a similar fashion, to investigate the impact of the disturbances on the current and voltage at the PCC, the converter of interest is considered as a short circuit. In doing so, the transfer matrices $\mathbf{N}_I(s)$ and $\mathbf{N}_V(s)$ are obtained, representing the frequency-domain mappings from the three-phase disturbance voltage $\mathbf{v}_{d,abc}$ to the PCC current $\mathbf{i}_{pcc,2,abc}$ and voltage $\mathbf{v}_{pcc,2,abc}$ due to disturbances, respectively, i.e.,

$$\mathbf{N}_I(s) = \mathcal{L}\{\mathbf{i}_{pcc,2,abc}\}(s) / \mathcal{L}\{\mathbf{v}_{d,abc}\}(s),$$

$$\mathbf{N}_V(s) = \mathcal{L}\{\mathbf{v}_{pcc,2,abc}\}(s) / \mathcal{L}\{\mathbf{v}_{d,abc}\}(s).$$

Finally, by applying the principle of superposition, the three-phase current and voltage at the PCC are expressed in the frequency domain by combining the contributions from both the converter output voltage and the disturbances. As a result, the PCC current is given by

$$\begin{aligned} \mathbf{i}_{pcc,abc}(s) &= \mathbf{i}_{pcc,1,abc}(s) + \mathbf{i}_{pcc,2,abc}(s) \\ &= \mathbf{M}_I(s) \mathbf{u}_{abc}(s) + \mathbf{N}_I(s) \mathbf{v}_{d,abc}(s), \end{aligned} \quad (1)$$

while the PCC voltage is

$$\begin{aligned} \mathbf{v}_{pcc,abc}(s) &= \mathbf{v}_{pcc,1,abc}(s) + \mathbf{v}_{pcc,2,abc}(s) \\ &= \mathbf{M}_V(s) \mathbf{u}_{abc}(s) + \mathbf{N}_V(s) \mathbf{v}_{d,abc}(s). \end{aligned} \quad (2)$$

By substituting s with $j n \omega_g$ —where ω_g is the grid angular frequency—the impact of the n^{th} voltage harmonic from the different sources on the n^{th} harmonic component of the PCC current and voltage can be determined for each harmonic order $n > 1$.

²For a detailed derivation of the state-space model, refer to [22].

B. Conventional OPPs

In a balanced three-phase system, it suffices to compute the 2π -periodic switching signal $u(\theta)$ for a single phase—e.g., $u_a(\theta) \equiv u(\theta)$ —since $u_b(\theta)$ and $u_c(\theta)$ can be obtained by phase-shifting $u(\theta)$. Signal $u(\theta)$ can have either quarter- and half-wave symmetry (QaHWS) or half-wave symmetry (HWS). Assuming QaHWS, the single-phase switching signal for a two-level converter is fully characterized by d switching angles (i.e., switching time instants) $\alpha_i \in [0, \pi/2]$, $i \in \{1, \dots, d\}$, within the first quarter of the fundamental period, and $d + 1$ switch positions u_j , $j \in \{0, 1, \dots, d\}$, with the initial switch position u_0 being either 1 or -1 . As a result, $u(\theta)$ can be represented by the Fourier series

$$u(\theta) = a_0 + \sum_{n=1}^{\infty} (a_n \cos(n\theta) + b_n \sin(n\theta)), \quad (3)$$

where all a_n Fourier coefficients are zero due to the QaHWS, while the b_n coefficients are nonzero only for odd harmonics and are given by

$$b_n = \frac{4u_0}{n\pi} \left(1 + 2 \sum_{i=1}^d (-1)^i \cos(n\alpha_i) \right), \quad n = 1, 3, 5, \dots \quad (4)$$

By contrast, a single-phase switching signal with HWS requires $2d + 1$ switching angles $\alpha_i \in [0, \pi]$, $i \in \{1, \dots, 2d + 1\}$, within the first half of the fundamental period. In this case, the nonzero a_n and b_n Fourier coefficients in (3) are given by

$$\begin{aligned} a_n &= -u_0 \frac{4}{n\pi} \sum_{i=1}^{2d+1} (-1)^i \sin(n\alpha_i), \quad n = 1, 3, 5, \dots, \\ b_n &= +u_0 \frac{4}{n\pi} \sum_{i=1}^{2d+1} (-1)^i \cos(n\alpha_i), \quad n = 1, 3, 5, \dots \end{aligned} \quad (5)$$

Given the above, and assuming zero harmonic disturbances at the PCC, conventional QaHWS OPPs can be computed for grid-connected converters with *LCL* filters. They aim to produce the minimum output current TDD, defined as

$$I_{\text{TDD}} = \frac{1}{\sqrt{2}I_{\text{nom}}} \sqrt{\sum_{n=5,7,\dots} \hat{i}_{\text{pcc},a,n}^2}, \quad (6)$$

with I_{nom} being the rms value of the nominal current, and $\hat{i}_{\text{pcc},a,n}$ the magnitude of the n^{th} phase-*a* current harmonic at the PCC. Note that triplen current harmonics ($n = 3, 9, \dots$) are not considered in (6), as they are zero in a balanced three-phase system with a floating star point.

Accordingly, the conventional QaHWS OPP optimization problem is formulated as

$$\underset{[\alpha_1 \dots \alpha_d]^T}{\text{minimize}} \quad \sum_{n=5,7,\dots} \left(\frac{g_n}{n} \left(1 + 2 \sum_{i=1}^d (-1)^i \cos(n\alpha_i) \right) \right)^2 \quad (7a)$$

$$\text{subject to } b_1 = m \quad (7b)$$

$$0 \leq \alpha_1 \leq \alpha_2 \leq \dots \leq \alpha_d \leq \frac{\pi}{2} \quad (7c)$$

$$u_0 \in \{-1, 1\}, \quad (7d)$$

where $m \in [0, 4/\pi]$ denotes the modulation index, and g_n is the gain from \mathbf{u}_{abc} to the PCC current for each harmonic of order $n = 6k \pm 1$, $k \in \mathbb{N}^+$. In addition, constraint (7c) ensures that the switching angles are in ascending order.

Even though (7) tailors OPPs to higher-order systems, it does not guarantee compliance with harmonic grid standards. This can be addressed by explicitly constraining the amplitudes of non-triplen odd PCC current and voltage harmonics to the maximum levels $\hat{i}_{n,\text{max}}$ and $\hat{v}_{n,\text{max}}$ allowed by the standards [1] and [2], respectively, i.e.,

$$\hat{i}_{\text{pcc},a,n} \leq \hat{i}_{n,\text{max}} \quad (8a)$$

$$\hat{v}_{\text{pcc},a,n} \leq \hat{v}_{n,\text{max}}. \quad (8b)$$

Nevertheless, the grid-friendly operation of the aforementioned harmonic-constrained OPPs may be compromised in the presence of harmonic disturbances at the PCC. Under such conditions, ensuring compliance with grid standards requires incorporating the impact of disturbances into the system model (see Section II-A). This was done in [22], but under the assumption that the disturbance profile—i.e., the exact frequency, magnitude, and phase of harmonics—was fully known. As this is typically not the case in practice, OPPs must be designed to ensure adherence to grid standards even when disturbances are unknown during the offline OPP computation. To this end, robust OPPs are introduced in the sequel.

C. Robust Harmonic-Constrained HWS OPPs That Account for Unknown Disturbances

It is assumed that the n^{th} phase-*a* disturbance voltage harmonic has a magnitude within the range $\hat{v}_{d,a,n} \in [0, \hat{v}_{n,\text{max}}]$ and an arbitrary phase $\phi_{d,a,n} \in [-\pi, \pi)$. To obtain robust OPPs, i.e., OPPs that ensure compliance with grid standards regardless of disturbances at the PCC, all possible magnitudes and phases must be considered for each harmonic of order $n = 6k \pm 1$, with $k \in \mathbb{N}_1 = \{1, \dots, 8\}$, i.e., the harmonics typically regulated by grid standards. Based on the considered magnitude and phase ranges, the uncertainty set Ξ_n is defined for each order n as a disk with radius $\hat{v}_{n,\text{max}}$. As each disk contains infinitely many points, it must be equidistantly sampled to ensure computational tractability, see Fig. 3.

Given the above, for each sampled combination of the magnitude and phase, the following system of nonlinear equations is solved to obtain the Fourier coefficients \tilde{a}_n and \tilde{b}_n of the n^{th} disturbance voltage harmonic

$$\begin{cases} \hat{v}_{d,a,n} = \sqrt{\tilde{a}_n^2 + \tilde{b}_n^2} \\ \phi_{d,a,n} = \arctan(\tilde{a}_n/\tilde{b}_n). \end{cases} \quad (9)$$

Using these coefficients, the phase-*a* disturbance voltage $v_{d,a}$ can be described by the Fourier series

$$v_{d,a}(\theta) = \sum_{n=1}^{\infty} \left(\tilde{a}_n \cos(n\theta) + \tilde{b}_n \sin(n\theta) \right). \quad (10)$$

It is important to note that, since the harmonic disturbances at the PCC are unknown, the coefficients \tilde{a}_n and \tilde{b}_n are treated

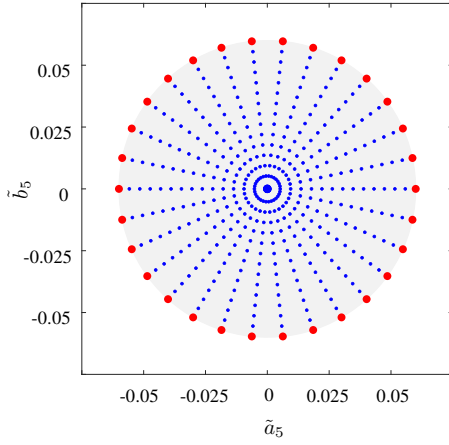


Fig. 3. Uncertainty realizations in the robust OPP problem for the 5th disturbance voltage harmonic at the PCC. The gray region illustrates the full uncertainty set Ξ_5 , with blue points denoting the equidistantly sampled realizations. Red points represent the realizations corresponding to the worst-case scenario, i.e., $\hat{\Xi}_5$.

as uncertainties in the OPP computation. For this reason, any combination of these coefficients is hereafter referred to as an “uncertainty realization”.

Nevertheless, accounting for all the aforementioned sampled points in Ξ_n significantly increases the size and complexity of the OPP optimization problem. To reduce the number of to-be-considered uncertainty realizations—without compromising robustness to disturbances—only those with the maximum allowable magnitude are retained for each harmonic order n , as they represent the most challenging scenario for compliance with grid standards. These uncertainty realizations form the set $\hat{\Xi}_n$ for each disturbance harmonic and span the entire circle of radius $\hat{v}_{n,\max}$, see, e.g., the red points in Fig. 3 for $n = 5$. The number of realizations in $\hat{\Xi}_n$ depends on the phase angle sampling resolution over $[-\pi, \pi)$.

To improve the robustness to harmonic disturbances, OPPs with HWS—rather than QaHWS—are considered as they allow adjusting the phases of the OPP harmonic components. Accordingly, given the Fourier coefficients a_n and b_n for HWS OPPs (see (5)) as well as \tilde{a}_n and \tilde{b}_n for disturbances, the amplitude of the n^{th} phase- a PCC current and voltage harmonics can be obtained with the help of (1) and (2), respectively, as

$$\hat{i}_{\text{pcc},a,n} = \left(\left(a_n Q_{1,n} + b_n Q_{2,n} + \tilde{a}_n Q_{3,n} + \tilde{b}_n Q_{4,n} \right)^2 + \left(-a_n Q_{2,n} + b_n Q_{1,n} - \tilde{a}_n Q_{4,n} + \tilde{b}_n Q_{3,n} \right)^2 \right)^{1/2} \quad (11a)$$

$$\hat{v}_{\text{pcc},a,n} = \left(\left(a_n Q_{5,n} + b_n Q_{6,n} + \tilde{a}_n Q_{7,n} + \tilde{b}_n Q_{8,n} \right)^2 + \left(-a_n Q_{6,n} + b_n Q_{5,n} - \tilde{a}_n Q_{8,n} + \tilde{b}_n Q_{7,n} \right)^2 \right)^{1/2}, \quad (11b)$$

where $Q_{\ell,n}$, with $\ell \in \{1, 2, \dots, 8\}$, depend on the entries of the matrices $M_I(s)$, $M_V(s)$, $N_I(s)$, and $N_V(s)$ for each

harmonic order n , see [22]. Moreover, using (11a) together with (6), the TDD of the current at the PCC is computed with

$$I_{\text{TDD}} = \frac{1}{\underbrace{\sqrt{2}I_{\text{nom}}}_c} \left(\sum_{n=5,7,\dots} \left(u_0 \frac{-4Q_{1,n}}{n\pi} \sum_{i=1}^{2d+1} (-1)^i \sin(n\alpha_i) + u_0 \frac{4Q_{2,n}}{n\pi} \sum_{i=1}^{2d+1} (-1)^i \cos(n\alpha_i) + \tilde{a}_n Q_{3,n} + \tilde{b}_n Q_{4,n} \right)^2 + \left(u_0 \frac{4Q_{2,n}}{n\pi} \sum_{i=1}^{2d+1} (-1)^i \sin(n\alpha_i) + u_0 \frac{4Q_{1,n}}{n\pi} \sum_{i=1}^{2d+1} (-1)^i \cos(n\alpha_i) - \tilde{a}_n Q_{4,n} + \tilde{b}_n Q_{3,n} \right)^2 \right)^{\frac{1}{2}}, \quad (12)$$

which is of the form $I_{\text{TDD}} = c\sqrt{J_{\text{HWS}}}$. By discarding the constant c —which does not influence the optimization— J_{HWS} serves as the objective function in the robust OPP optimization problem.

Given the above, the proposed robust harmonic-constrained OPPs are computed by solving a min-max optimization problem that accounts for the uncertainty realizations in $\hat{\Xi}_n$ for all harmonics of order $n = 6k \pm 1, k \in \mathbb{N}_1$. Specifically, the proposed robust OPP problem is formulated as

$$\underset{\alpha_H, \epsilon}{\text{minimize}} \quad \max_{\xi_n \in \hat{\Xi}_n} (J_{\text{HWS}} + \epsilon^T \mathbf{W} \epsilon) \quad (13a)$$

$$\text{subject to} \quad b_1 = m \quad (13b)$$

$$a_1 = 0 \quad (13c)$$

$$0 \leq \alpha_1 \leq \alpha_2 \leq \dots \leq \alpha_{2d+1} \leq \pi \quad (13d)$$

$$\hat{i}_{\text{pcc},a,n} \leq \hat{i}_{n,\max} + \epsilon_{i,n}, \quad \epsilon_{i,n} \geq 0, \quad \forall n = 6k \pm 1, k \in \mathbb{N}_1, \forall \xi_n \in \hat{\Xi}_n \quad (13e)$$

$$\hat{v}_{\text{pcc},a,n} \leq \hat{v}_{n,\max} + \epsilon_{v,n}, \quad \epsilon_{v,n} \geq 0, \quad \forall n = 6k \pm 1, k \in \mathbb{N}_1, \forall \xi_n \in \hat{\Xi}_n \quad (13f)$$

$$u_0 \in \{1, -1\}. \quad (13g)$$

In the above problem, (13b) and (13c) synthesize the fundamental OPP component with amplitude $m \in [0, 4/\pi]$ and zero phase. In addition, constraints (13e) and (13f) are imposed to keep the amplitude of the PCC current and voltage harmonics within the limits specified by standards [1] and [2], respectively. These constraints are enforced for all uncertainty realizations in $\hat{\Xi}_n$, for each $n = 6k \pm 1, k \in \mathbb{N}_1$. For example, for the 5th harmonic, $\hat{i}_{\text{pcc},a,5}$ and $\hat{v}_{\text{pcc},a,5}$ are constrained for all the red points shown in Fig. 3. Notably, the Fourier coefficients \tilde{a}_n and \tilde{b}_n corresponding to these realizations in $\hat{\Xi}_n$ are aggregated into the vector $\xi_n = [\tilde{a}_n^T \tilde{b}_n^T]^T$.

Finally, it is worth noting that the harmonic constraints are implemented as soft constraints in (13) to avoid feasibility issues associated with hard constraints. This is achieved by introducing the slack variables $\epsilon = [\epsilon_i^T \epsilon_v^T]^T$, where ϵ_i and ϵ_v comprise the current $\epsilon_{i,n}$ and voltage $\epsilon_{v,n}$ slack variables,

Algorithm 1 Computation of two-level robust OPPs

- 1: Given the desired number d of switching angles
- 2: Given an equidistantly gridded modulation interval $m \in [0, \frac{4}{\pi}]$, e.g., $m = 0 : \frac{1}{64\pi} : \frac{4}{\pi}$
- 3: Given an equidistantly gridded phase angle range of disturbances $\phi_{d,a,n} \in [-\pi, \pi)$, e.g., $\phi_{d,a,n} = -\pi : \frac{2\pi}{30} : \pi$
- 4: **for** each $n = 6k \pm 1, k \in \mathbb{N}_1$, **do**
- 5: **for** each combination of magnitude $\hat{v}_{d,a,n} = \hat{v}_{n,\max}$ and sampled phase angles $\phi_{d,a,n}$ **do**
- 6: Solve the system of nonlinear equations (9)
- 7: **end for**
- 8: **return** the set $\hat{\xi}_n$ of the uncertainty realizations corresponding to the worst-case scenario
- 9: **end for**
- 10: **for** each m **do**
- 11: **for** each combination of most challenging realizations, for all $n = 6k \pm 1, k \in \mathbb{N}_1$, in the objective function **do**
- 12: **for** each possible initial switch position u_0 **do**
- 13: Solve the OPP optimization problem (13) multiple times using the Matlab function `fmincon`, each time with a randomly initialized set of $2d + 1$ initial angles
- 14: **end for**
- 15: **return** the initial switch position and corresponding switching angles that result in the minimum I_{TDD}
- 16: **end for**
- 17: **return** the initial switch position u_0^* and corresponding switching angles α_H^* that yield the maximum I_{TDD} due to the most challenging combination of realizations
- 18: **end for**

respectively, for $n = 6k \pm 1, k \in \mathbb{N}_1$. Nevertheless, to facilitate compliance with grid standards, potential violations of these soft constraints are heavily penalized in the objective function via the (diagonal) weighting matrix \mathbf{W} . It is noteworthy that the slack variables ϵ , together with the switching angles $\alpha_H = [\alpha_1 \dots \alpha_{2d+1}]^T$, constitute the optimization variables of problem (13). The procedure for computing the proposed robust OPPs is described in Algorithm 1.

III. NUMERICAL RESULTS

This section assesses the performance of the proposed robust OPPs, computed with (13), in the presence of harmonic disturbances at the PCC, and compares them with conventional (unconstrained) QaHWS OPPs (see problem 7) and SHE. The pulse patterns are computed for the LV system depicted in Fig. 1, which comprises a converter rated at 12.5 kVA with a dc-link voltage of 650 V, and an *LCL* filter with a resonance frequency of 957 Hz. The rated values and system

TABLE I
RATED VALUES OF THE SYSTEM

Parameter	Symbol	SI Value
Voltage	V_R	400 V
Current	I_R	18 A
Angular grid frequency	ω_{gR}	$2\pi 50$ rad/s
Short-circuit ratio	k_{sc}	13.6
Grid impedance ratio	k_{XR}	7

TABLE II
SYSTEM PARAMETERS

Grid	Inductance	L_g	3 mH
	Resistance	R_g	136 m Ω
Other converters	Transformer inductance	L_l	3.1 mH
	Transformer resistance	R_l	137.5 m Ω
<i>LCL</i> filter	Converter-side inductance	L_{fc}	6.6 mH
	Converter-side resistance	R_{fc}	100 m Ω
	Capacitance	C	8.8 μ F
	Capacitor resistance	R_c	0.8 m Ω
	Grid-side inductance	L_{fg}	6 mH
	Grid-side resistance	R_{fg}	70 m Ω

parameters are provided in Tables I and II, respectively. The chosen operating point corresponds to a modulation index of $m = 1.0785$, and an OPP with $d = 10$ is considered, resulting in a switching frequency of $f_{sw} = 1050$ Hz. Moreover, the SHE method aims to eliminate all non-triplen odd harmonics in the range $n \in [5, 29]$.

To quantify the degree of compliance with the relevant harmonic grid standards and enable meaningful comparisons, the following current I_m and voltage V_m metrics are introduced, where lower values indicate better performance:

$$I_m = \frac{1}{2|\mathbb{N}_1|} \sum_{n=5,7,\dots,49} \frac{\max_{\xi_n \in \hat{\xi}_n} (\hat{i}_{pcc,a,n} - \hat{i}_{n,\max})}{\hat{i}_{n,\max}}$$

$$V_m = \frac{1}{2|\mathbb{N}_1|} \sum_{n=5,7,\dots,49} \frac{\max_{\xi_n \in \hat{\xi}_n} (\hat{v}_{pcc,a,n} - \hat{v}_{n,\max})}{\hat{v}_{n,\max}}$$

Note that $2|\mathbb{N}_1| = 16$ denotes the number of non-triplen odd harmonics over which constraints (13e) and (13f) are imposed in the OPP optimization problem (13).

When the proposed OPPs are computed for the worst-case scenario—i.e., the 5th to 49th non-triplen odd disturbance harmonics with maximum magnitudes as specified by [2]—it is not possible to keep all PCC current and voltage harmonics within the desired limits. This is due to the lack of information about the disturbance phases, which prevents effective adjustment of the OPP harmonic phases to mitigate their impact.

As it turns out, to ensure full compliance with both current and voltage harmonic grid standards, the magnitude of the disturbance voltage harmonics must be limited to 55% of the maximum values allowed by [2], regardless of phase. For this disturbance harmonic profile (see Fig. 4(a)), the proposed OPPs are compared to the conventional OPPs and SHE in

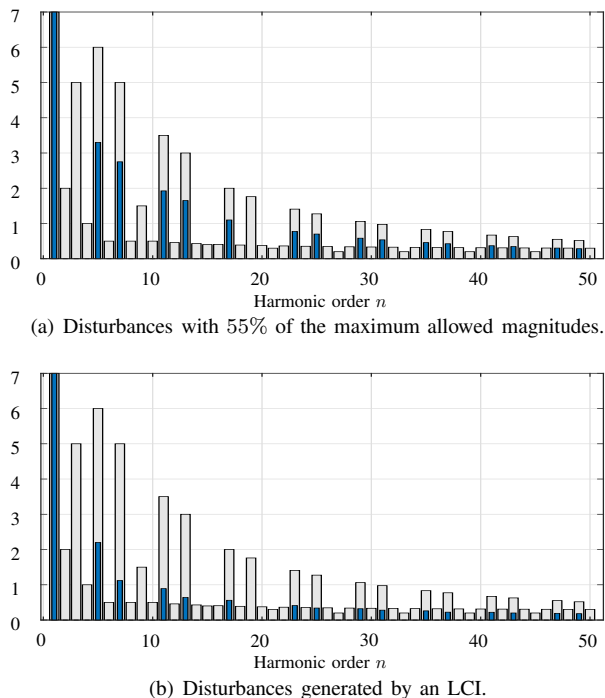


Fig. 4. Harmonic voltage disturbances at the PCC (%) (a) with 55% of the maximum allowed magnitudes, (b) generated by an LCI. The grid standard limits are shown as light gray bars, and harmonic disturbances are shown as blue bars.

Fig. 5. Note that the 19th disturbance harmonic—i.e., the harmonic close to the filter resonance frequency—is assumed to be attenuated by a controller. In addition, for each n , the maximum values of the PCC current and voltage harmonics are reported, considering all possible disturbance phases. As shown, the proposed OPPs ensure full compliance, whereas both the conventional OPPs and SHE-based pulse patterns result in violations of the harmonic grid standards for both PCC current and voltage harmonics. This is reflected in the high values of the introduced performance metrics, namely $I_m = 17.36$ and $V_m = 11.05$ for the conventional OPPs, and $I_m = 30.11$ and $V_m = 16.23$ for SHE.

To evaluate the performance in a realistic scenario, a three-phase line-commutated inverter (LCI) is assumed to be connected at the PCC. In the presence of harmonic disturbances introduced by the LCI (see Fig. 4(b)), the harmonic spectra produced by the benchmarked PWM methods at the PCC are illustrated in Fig. 6. As observed, the proposed robust OPPs ensure adherence to the voltage and current harmonic limits, even though the LCI-generated disturbances are unknown during the OPP computation. As a result, the introduced performance metrics yield $I_m = 0$ and $V_m = 0$. In contrast, both conventional OPPs and SHE-based pulse patterns result in several violations of the relevant harmonic grid standards, as indicated by the non-zero values, i.e., $I_m = 10.93$ and $V_m = 1.78$ for the conventional OPPs, and $I_m = 22.92$ and $V_m = 11.11$ for SHE.

Therefore, the proposed robust OPPs achieve better compliance with harmonic grid standards than existing PWM

methods, regardless of the harmonic content injected into the PCC by other converters. However, this favorable performance of the proposed robust OPPs at the individual harmonic level comes at the expense of increased current and voltage TDDs. This is because the computed OPPs are conservative since they are computed to guarantee compliance under a completely unknown disturbance profile. Specifically, without knowledge of the disturbance phases—which necessitates considering all phase angles in $[-\pi, \pi)$ —the phase of the OPP harmonics cannot be optimally adjusted to counteract the disturbances.

IV. DISCUSSION

As demonstrated in Section III, the proposed robust OPPs exhibit superior performance in ensuring compliance with harmonic grid standards—an essential requirement for grid-connected converters. Although these OPPs are designed to be robust against harmonic disturbances at the PCC, certain challenges exist. Notably, as discussed in Section III, achieving full compliance is feasible only when the magnitudes of the considered non-zero disturbance harmonics remain within 55% of the maximum levels permitted by standards. This limitation arises from the fact that the disturbance profile—especially the phase information—is unavailable during the offline computation of the OPPs. As a result, under entirely unknown disturbances, designing pulse patterns that guarantee grid-friendly operation across all scenarios becomes extremely difficult, if not impossible.

In addition, incorporating robustness into the OPP optimization problem inherently restricts the solution space, particularly since all possible phase angles of disturbance harmonics need to be considered. This gives rise to a trade-off between meeting harmonic limits and low TDD values, thus resulting in higher current and voltage TDDs when ensuring compliance under the worst-case scenarios. Moreover, such robustness often results in conservatism, i.e., OPPs designed for the worst case may yield suboptimal TDDs under less demanding operating conditions.

To overcome these challenges, and achieve optimal performance across a wider range of scenarios, one possible approach is to compute multiple robust OPPs for different ranges of disturbance magnitudes and/or phases. Although this approach increases the required computational effort and time, its offline nature makes it manageable. However, storing the resulting OPPs in lookup tables (LUTs) for use in real time significantly increases memory requirements, thus challenging the real-time implementation of such a strategy. In cases with limited memory resources, learning-based techniques, such as artificial neural networks, may offer a viable alternative for enabling adaptive, real-time OPP generation [21].

V. CONCLUSIONS

This paper presented a method for computing two-level OPPs for grid-connected converters with *LCL* filters in the presence of unknown harmonic disturbances at the PCC. To ensure compliance with grid standards, a robust harmonic-constrained OPP optimization problem was formulated, ac-

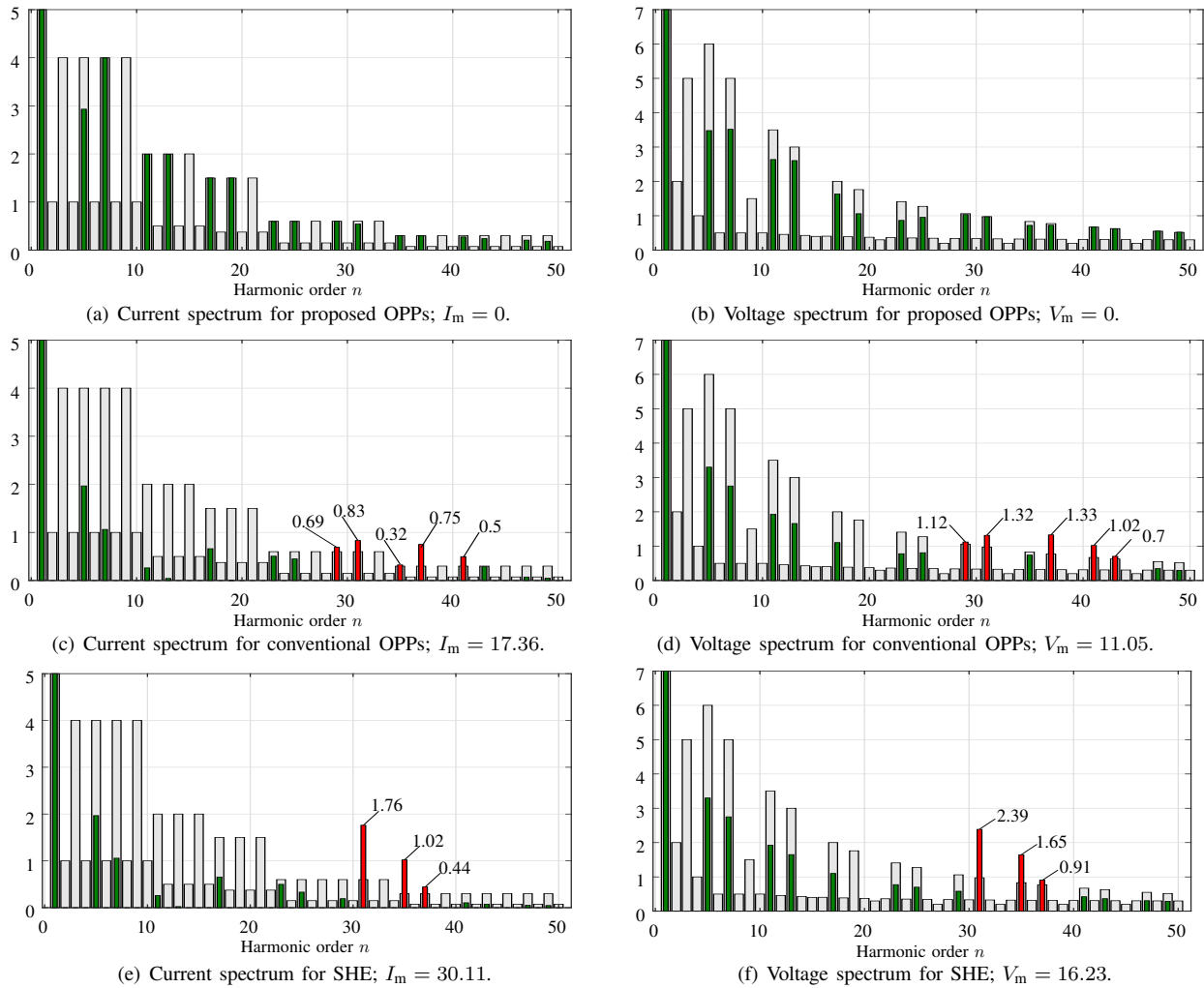


Fig. 5. Current and voltage harmonics at the PCC (%) for harmonic voltage disturbances with 55% of the maximum allowed magnitudes. The grid standard limits are shown as light gray bars, harmonics that meet them are shown as green bars, and harmonics that violate them are shown as red bars.

counting for the worst-case disturbance magnitudes and all possible phase angles. This was facilitated by adopting HWS for the switching signals, thus providing more degrees of freedom in the OPP optimization problem. Thanks to the proposed robust PWM framework, as shown by the presented results, compliance with harmonic grid standards is guaranteed under harmonic disturbances at the PCC with magnitudes up to 55% of the maximum allowed levels. As a result, the proposed OPPs achieve grid-friendly performance in terms of compliance with harmonic grid standards, in contrast to conventional OPPs and SHE.

ACKNOWLEDGMENT

This work was supported by the Research Council of Finland.

REFERENCES

- [1] IEEE Std 519-2014 (Revision of IEEE Std 519-1992), "IEEE recommended practices and requirements for harmonic control in electrical power systems," pp. 1–29, Jun. 2014.
- [2] IEC Std 61000-2-4, "Electromagnetic compatibility (EMC)—part 2-4: Environment—compatibility levels in industrial plants for low-frequency conducted disturbances," Sep. 2002.
- [3] I. Ibanez-Hidalgo, R. H. Cuzmar, A. Sanchez-Ruiz, A. Perez-Basante, A. Zubizarreta, S. Ceballos, and R. P. Aguilera, "Enhanced PI control based SHC-PWM strategy for active power filters," *IEEE Open J. Ind. Electron. Soc.*, vol. 5, pp. 1174–1189, Oct. 2024.
- [4] B. Singh, K. Al-Haddad, and A. Chandra, "A review of active filters for power quality improvement," *IEEE Trans. Ind. Electron.*, vol. 46, no. 5, pp. 960–971, Oct. 1999.
- [5] L. A. Moran, J. W. Dixon, and R. R. Wallace, "A three-phase active power filter operating with fixed switching frequency for reactive power and current harmonic compensation," *IEEE Trans. Ind. Electron.*, vol. 42, no. 4, pp. 402–408, Aug. 1995.
- [6] D. Bernet, L. Stefanski, and M. Hiller, "Integrating voltage-source active filters into grid-connected power converters—modeling, control, and experimental verification," *IEEE Trans. Power Electron.*, vol. 36, no. 11, pp. 12 218–12 233, Apr. 2021.
- [7] P. Acuña, L. Morán, M. Rivera, J. Dixon, and J. Rodriguez, "Improved active power filter performance for renewable power generation systems," *IEEE Trans. Power Electron.*, vol. 29, no. 2, pp. 687–694, Apr. 2014.
- [8] H. S. Patel and R. G. Hoft, "Generalized techniques of harmonic elimination and voltage control in thyristor inverters: Part I—Harmonic elimination," *IEEE Trans. Ind. Appl.*, vol. IA-9, no. 3, pp. 310–317, May/Jun. 1973.
- [9] W. Fei, X. Du, and B. Wu, "A generalized half-wave symmetry SHE-

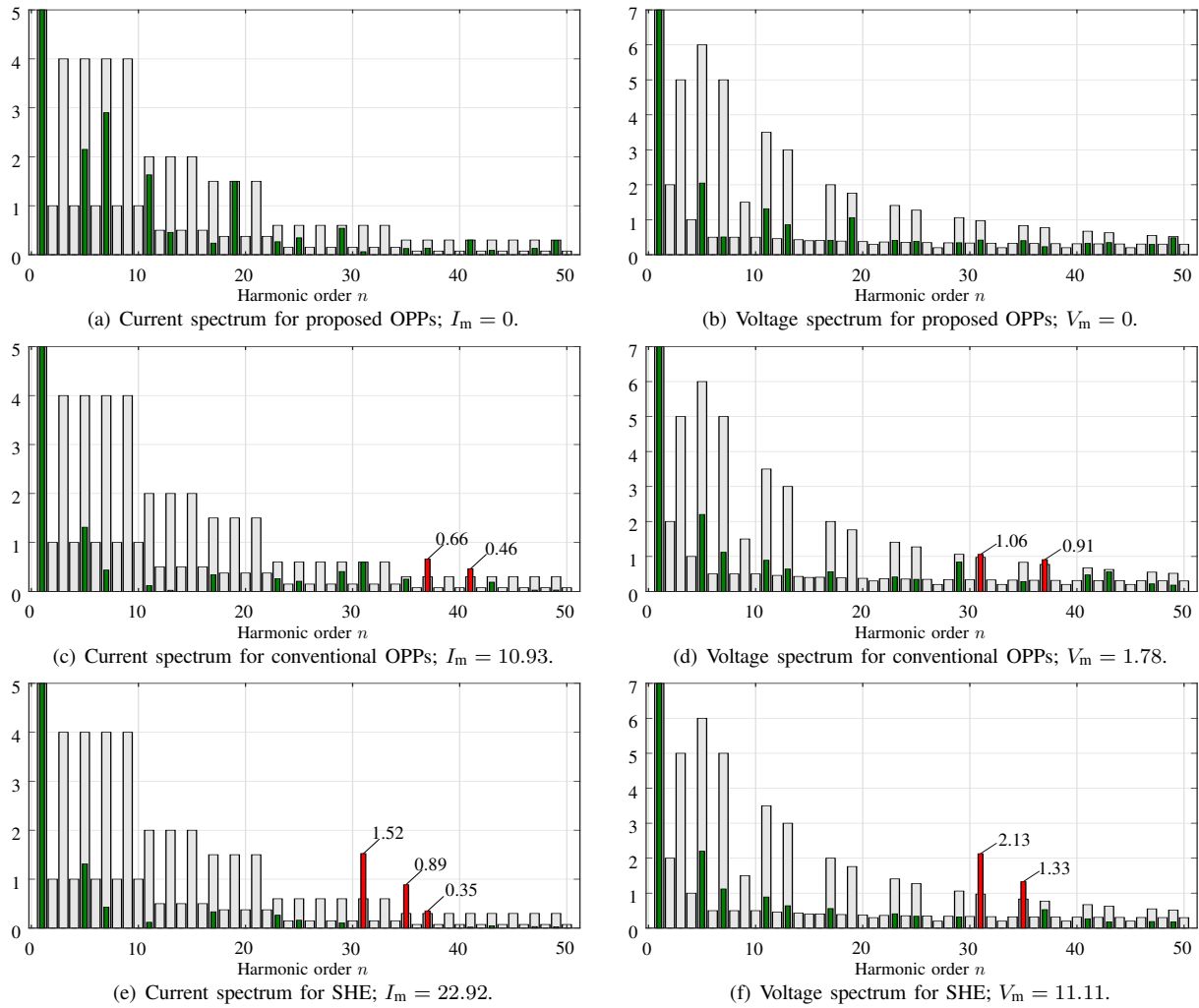


Fig. 6. Current and voltage harmonics at the PCC (%) for disturbances generated by an LCI. The grid standard limits are shown as light gray bars, harmonics that meet them are shown as green bars, and harmonics that violate them are shown as red bars.

PWM formulation for multilevel voltage inverters,” *IEEE Trans. Ind. Electron.*, vol. 57, no. 9, pp. 3030–3038, Sep. 2010.

[10] M. S. A. Dahidah, G. Konstantinou, and V. G. Agelidis, “A review of multilevel selective harmonic elimination PWM: Formulations, solving algorithms, implementation and applications,” *IEEE Trans. Power Electron.*, vol. 30, no. 8, pp. 4091–4106, Aug. 2015.

[11] J. Nápoles, J. I. Leon, R. Portillo, L. G. Franquelo, and M. A. Aguirre, “Selective harmonic mitigation technique for high-power converters,” *IEEE Trans. Ind. Electron.*, vol. 57, no. 7, pp. 2315–2323, Jul. 2010.

[12] G. S. Buja, “Optimum output waveforms in PWM inverters,” *IEEE Trans. Ind. Appl.*, vol. IA-16, no. 6, pp. 830–836, Nov./Dec. 1980.

[13] A. Birda, J. Reuss, and C. M. Hackl, “Synchronous optimal pulsewidth modulation for synchronous machines with highly operating point dependent magnetic anisotropy,” *IEEE Trans. Ind. Electron.*, vol. 68, no. 5, pp. 3760–3769, May 2021.

[14] L. G. Franquelo, J. Nápoles, R. C. P. Guisado, J. I. León, and M. A. Aguirre, “A flexible selective harmonic mitigation technique to meet grid codes in three-level PWM converters,” *IEEE Trans. Ind. Electron.*, vol. 54, no. 6, pp. 3022–3029, Dec. 2007.

[15] A. K. Rathore, J. Holtz, and T. Boller, “Synchronous optimal pulsewidth modulation for low-switching-frequency control of medium-voltage multilevel inverters,” *IEEE Trans. Ind. Electron.*, vol. 57, no. 7, pp. 2374–2381, Jul. 2010.

[16] J. A. Pontt, J. R. Rodriguez, A. Liendo, P. Newman, J. Holtz, and J. M. S. Martin, “Network-friendly low-switching-frequency multipulse high-power three-level PWM rectifier,” *IEEE Trans. Ind. Electron.*, vol. 56, no. 4, pp. 1254–1262, Apr. 2009.

[17] T. Geyer, P. Karamanakos, and I. Koukoulá, “Optimized pulse patterns with bounded semiconductor losses,” *IEEE Trans. Power Electron.*, vol. 39, no. 3, pp. 3233–3243, Mar. 2024.

[18] T. Dorfling, H. d. T. Mouton, and T. Geyer, “Generalized model predictive pulse pattern control based on small-signal modeling—Part 2: Implementation and analysis,” *IEEE Trans. Power Electron.*, vol. 37, no. 9, pp. 10488–10498, Sep. 2022.

[19] S. Rahmanpour, P. Karamanakos, and T. Geyer, “Harmonic-constrained three-level optimized pulse patterns for grid-connected converters with *LCL* filters,” *IEEE Trans. Ind. Appl.*, pp. 1–12, 2025, in press.

[20] A. Moeini, H. Zhao, and S. Wang, “A current-reference-based selective harmonic current mitigation PWM technique to improve the performance of cascaded H-bridge multilevel active rectifiers,” *IEEE Trans. Ind. Electron.*, vol. 65, no. 1, pp. 727–737, Jan. 2018.

[21] I. Ibanez-Hidalgo, A. Sanchez-Ruiz, A. Perez-Basante, A. Zubizarreta, S. Ceballos, S. Gil-Lopez, and R. P. Aguilera, “Real time selective harmonic control—PWM based on artificial neural networks,” *IEEE Trans. Power Electron.*, vol. 39, no. 1, pp. 768–783, Jan. 2024.

[22] S. Rahmanpour, P. Karamanakos, and T. Geyer, “Optimized pulse patterns for converters connected to a distorted grid via *LCL* filters,” in *Proc. IEEE Energy Convers. Congr. Expo. Europe*, Darmstadt, Germany, Sep. 2024, pp. 1–8.